Impact of Acquisition Time-window on Clinical Whole-body PET Parametric Imaging

Nicolas A. Karakatsanis[1,2], *Member, IEEE*, Martin A. Lodge[2], Michael E. Casey[3], Habib Zaidi[1,4,5], *Senior Member, IEEE* and Arman Rahmim[2,6], *Senior Member, IEEE*

***Abstract*– Whole-body PET parametric imaging can combine the benefit of extended axial field-of-view (FOV) in multi-bed scans with that of generating time activity curves (TACs) in dynamic scans. We have recently proposed such a framework capable of delivering whole-body FDG Patlak images in clinically feasible scan times. The design of the acquisition protocol was limited to a single time-window and the standard Patlak graphical analysis method. However, the relatively long FDG half-life and uptake, compared to clinically acceptable acquisition time-windows, render the choice of this window critical. The major FDG kinetic components can be estimated from the early and intermediate TAC segments. On the contrary, at later time-windows, tumor contrast may be overall higher. In addition, the standard Patlak method does not account for tracer uptake reversibility, a property that becomes more apparent at later acquisition time-windows for certain tumors, thus increasing the probability for larger bias at later times. Consequently, the choice of the optimal time-window can be critical and should constitute an important design aspect of multi-bed dynamic protocols. In the present work we assessed the impact of a sliding acquisition time-window on whole-body FDG PET parametric images. This included incremental shift of a 6-pass acquisition time-window (~35min) along an extended scan period of 0-90min post injection, using both real patient kinetic data as well as realistic 4D simulations of the state-of-the-art Siemens Biograph mCT scanner. We also propose the selective application of a generalized Patlak method accounting for uptake reversibility. Our simulated and clinical results demonstrate that both Patlak methods (standard and generalized) result in enhanced tumor-to-background contrast as well as contrast-to-noise ratios with minimal bias at an early acquisition time window (10-45min post injection) with the generalized method exhibiting systematically superior performance.**

I. INTRODUCTION

DYNAMIC PET imaging allows for the acquisition of tracer time activity curves (TACs) enabling estimation of kinetic parameter at the voxel level (parametric imaging) [1-10]. However, its application has been limited to research setting. Recently, we proposed a clinically feasible multi-bed dynamic PET imaging framework for FDG tracers, coupled with Patlak-based kinetic models and indirect as well as direct kinetic parametric image reconstruction methods, to facilitate its transition to the clinic for tumor detection and quantification [11-14].

The design of the scan protocol of the proposed framework was restricted to an acquisition time-window starting always right after the completion of an early dynamic heart scan 0-6-mins post-injection [11,15]. In addition, only the standard Patlak model was considered [16]. However, the choice of the time position of this acquisition window, relative to injection time, may be critical for the contrast and noise properties of the final clinical parametric PET images, due to

1) the considerably long time range during which the kinetics of FDG and other ^{18}F tracers are usually expressed in human normal tissues and tumors [1,4,7,17], and
2) the long ^{18}F half-life (110 mins).

These two properties of FDG kinetics result in relatively slowly changing TACs implying an extensive time spread of the kinetic information over a large time period after injection in comparison to the maximum acquisition time windows of ~30mins that are nowadays usually accepted in clinical routine when considering patient throughput and comfort criteria [1,17]. Consequently, large dynamic acquisition time periods are often required to sufficiently estimate the full kinetic properties of FDG in tissues and suspected tumor regions. However, after conducting an optimization analysis study, we proposed limiting the length of the acquisition time window to only 6 whole-body dynamic passes across all beds of the whole-body field of view (FOV) or equivalently to 30-35min, in order to conform to the routine clinical PET study requirements [15]. In addition, whole-body dynamic PET acquisitions inherently contain large time gaps of ~6min between the frames of each bed, thus, further limiting the time period for which actual data acquisition occurs [11].

Therefore, in this study, to maximize the amount of kinetic information that can possibly be acquired from a dynamic whole body PET scan within a given scan time-window, already optimized in terms of its time length, we:

a) additionally optimize the position, relative to injection, of the acquisition time-window, and
b) comparatively investigate the impact of the window position for two previously proposed Patlak graphical analysis methods, each using different assumptions for the tracer uptake reversibility [18,19].

This work was supported by the Swiss National Science Foundation under Grant SNSF 31003A-149957 and by Siemens Medical Solutions.

[1] N. A. Karakatsanis (e-mail: nikolaos.karakatsanis@unige.ch) and H. Zaidi are with the Division of Nuclear Medicine and Molecular Imaging, School of Medicine, University of Geneva, Geneva, Switzerland

[2] N. A. Karakatsanis is also together with M. A. Lodge and A. Rahmim with the Department of Radiology, School of Medicine, Johns Hopkins University, Baltimore, MD, USA

[3] M. E. Casey is with Siemens Medical Solutions, Knoxville, TN, USA

[4] H. Zaidi is also with Geneva Neuroscience Centre, University of Geneva, Geneva, Switzerland

[5] H. Zaidi is also with the Department of Nuclear Medicine and Molecular Imaging, University of Groningen, Groningen, Netherlands

[6] A. Rahmim is also with the Department of Electrical & Computer Engineering, Johns Hopkins University, Baltimore, MD, USA.

978-1-4799-6097-2/14/$31.00 ©2014 IEEE

The FDG tracer kinetics may result in considerable changes of the count and contrast levels in both suspected tumors and their background regions, especially in the early frames, where the rise of the TAC is steep with time [1,11]. In addition, it has been shown that FDG may exhibit in some tumor or normal tissue regions a small, but non-negligible, tracer uptake reversibility, whose net tracer efflux effect can be modeled by the kinetic macro-parameter (k_{loss}) or tracer efflux rate constant and is linearly dependent on k_4 kinetic micro-parameter [18-21]. Tracer uptake reversibility, or k_{loss}, is expected to reduce, though to a relatively small extent, the absorbed or metabolized amount of activity, with the apparent effect on TACs being negligible at early frames but gradually becoming stronger at later time frames or TAC segments [19-21].

The standard Patlak method does not account for k_{loss} effect, i.e. erroneously assumes it is zero, resulting in underestimation of the estimated tracer influx rate parameter K_i in regions with non-negligible uptake reversibility [18-21], with the bias becoming larger for stronger underlying k_{loss} rate constants [16,18,19]. However, this model supports a linear graphical analysis method and, thus, it is very robust to noise. On the other hand, a generalized Patlak method had been also introduced to additionally support k_{loss} modeling for more quantitative estimation of K_i parametric images, at the cost of smaller tolerance to noise, due to the non-linear estimation process involved [19].

Both of the above-mentioned tasks, (a) and (b), are equally important in this impact evaluation study, as they are expected to affect each other. The choice of a particular time-window position can impact the quality of parametric images but this effect may be different between the two examined Patlak models. This is because each model is associated with: 1) different k_{loss} assumptions and 2) different robustness to the high noise levels usually present in whole-body dynamic PET data.

Our aim in this study is to provide, through a systematic and quantitative evaluation of parametric images, a sufficient answer to the following question: When is the best time to acquire a set of 6 passes of whole-body FDG PET data after injection and how the choice of different Patlak models can affect our decision? By investigating this problem, we hope to derive conclusions that would further facilitate the smoother clinical adoption of this quantitative PET imaging framework in the clinic.

II. Methods and Materials

In this study we systematically investigate the quantitative impact of acquisition time-window position on whole-body PET parametric images for two previously introduced Patlak estimation methods. For that purpose, we evaluate the effect of an incremental shift of an already optimized fixed-length acquisition time-window along a unique dynamic whole-body PET dataset of 0-90min post injection, using both real patient kinetic data as well as realistic 4D simulations of state-of-the-art Siemens Biograph mCT TOF PET scanner [22] with kinetic parameter values obtained from literature (Table I) [23-25].

TABLE I. K Rate Parameters

Regions	K_1	k_2	k_3	k_4	V_B
Normal Liver	0.864	0.981	0.005	0.016	-
Liver Tumor	0.243	0.78	0.1	0	-
Normal Lung	0.108	0.735	0.016	0.013	0.017
Liver Tumor 2	0.283	0.371	0.057	0.012	-
Myocardium	0.6	1.2	0.1	0.001	-

A. Sliding acquisition time window

The time course of activity concentration during the first 90min after injection of FDG or other F-18 tracers typically exhibits considerable variation in many uptake regions [1,11]. However, the available time window for clinical acquisition is limited. Thus, a challenge arises in selecting which time segment of the TACs better characterizes the overall kinetics of the tracer across all voxels of the primary regions of interest. That choice is also affected by the kinetic model. Consequently, the selection of the appropriate time-window for the employed kinetic model should constitute an important specification of any single- or multi-bed dynamic acquisition protocol. Previously, we proposed a multi-bed dynamic PET acquisition scheme, consisting of two separate phases [11]:

a) an initial 6-min dynamic scan over the heart bed to acquire the early segment of the input function, i.e. the TAC in blood plasma, followed by
b) a dynamic series of unidirectional whole-body passes, each consisting of bed frames of equal duration (45sec), to acquire the later portion of the input function as well as of the TACs of all voxels in all beds.

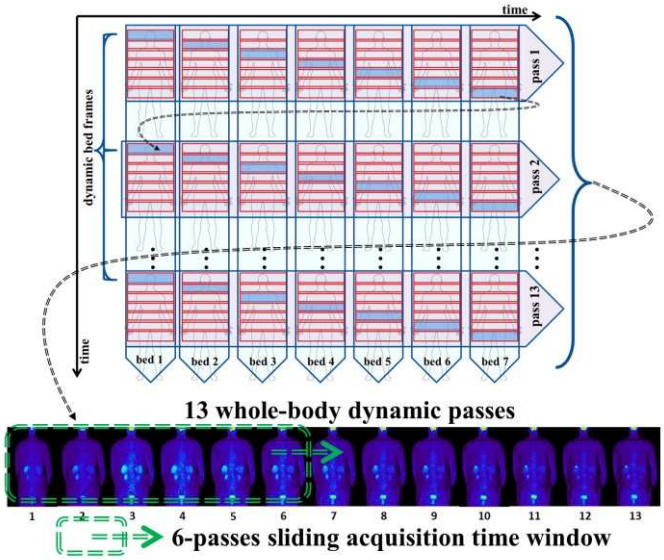

Fig. 1. Schematic representation of the second phase of whole body dynamic acquisition sequence and the direction of shift of the 6-frame acquisition window across the 13 passes collected from 0-90min post-injection.

In the current study, we focus on the second phase and consider a range of shifted acquisition time windows, with respect to the injection time. The utilized time window consists of 6 whole-body passes, each comprised of 7 beds, each scanned for 45sec. Its total duration is ~35mins with

initial time positioning corresponding right after the completion time of the first acquisition phase [11,15]. The remaining time positions can be derived by gradually shifting the window to later times always by an interval equal to the time period of a single pass. After accounting for the bed positioning capabilities of modern PET scanners and confirming with an actual clinical whole body scan, we concluded that at least a total of 13 such wholebody passes can be completed within a 0-90min time period [22].

B. Standard and generalized Patlak graphical analysis method

The selection of the appropriate kinetic model can be critical for a dynamic PET study, as each model makes certain assumptions for the underlying tracer kinetics and accordingly determines, through its model equation, which quantitative physiological parameters it can directly estimate and what type of dynamic activity measurements are needed for that purpose [26,27]. In addition, the model equation can relate the dynamic activity measurements with the estimated physiological parameters in a linear or non-linear manner, the latter being the case for more descriptive models with higher number of parameters to be estimated and overall complexity, thus, affecting the estimation process robustness to noise [12,18,19]. Therefore, the kinetics of the tracer and the data acquisition protocol can drastically limit the choice of appropriate kinetic models applicable to a particular dynamic PET study.

Our proposed framework of dynamic whole-body FDG PET acquisitions requires the sampling of the TACs for all the voxels of all bed positions across the body. The need to acquire dynamic data across multiple beds introduces relatively large time gaps between subsequent dynamic frames of each bed, proportional to the scan time per bed. As a result, given a minimum scan period of ~20sec at each bed to acquire sufficient count statistics, any rapid changes of activity cannot be practically captured in multi-bed dynamic PET acquisitions. Therefore, for our proposed protocol to be clinically feasible, it has to consist of the two acquisition phases described in section A: the early 6-min dynamic scan over the heart bed serves only for tracking the rapidly changing early section of the heart ventricles TAC (input function), while the time series of 6 whole-body passes, each lasting for ~6min, aims in sufficiently capturing the later slowly changing portion of all voxel TACs across all beds.

Consequently, the early 6-min section of all voxel TACs, except from those belonging to the heart bed, is missing. Thus, kinetic models or graphical analysis methods requiring time sampling of the whole section of TAC, i.e. starting from injection time (fully compartmental kinetic model, Logan method etc), at every voxel cannot be practically applied in the context of clinical whole-body PET FDG parametric imaging with current PET scanner hardware and software technology available today [26-28].

On the other hand, the class of graphical analysis methods based on Patlak modeling formulation, such as the standard Patlak analysis method, are well suited for voxel-based estimation of the tracer influx rate constant K_i by only requiring [11,16,18,19]:

a) the time activity measurements from only the later sections (>7-min) of all voxel TACs across beds and
b) the time integral of the input function, which is common after certain delay and dispersion corrections, for all voxels and can be measured from the heart bed.

The model equation for the standard Patlak model relates the activity concentration PET measurements in the blood plasma $C_p(t)$ (input function) and the tissue voxels $C(t)$ at the frame corresponding to time t, relative to injection, with the unknown physiological or kinetic parameters of tracer net influx rate constant K_i and total blood distribution volume V, as follows [16]:

$$\begin{aligned} \mathrm{C(t)} &= K_i \int_0^t C_p(t)d\tau + VC_p(t) \\ &= K_i * C_p(t) + VC_p(t),\ t > t^* \end{aligned} \quad (1)$$

where $*$ denotes the operation of convolution and t^* is the time at which relative equilibrium is attained between the concentration of tracer in blood plasma and that of non-metabolized tracer in tissue [16]. In this study, we focus on the estimation of K_i images, because of their high clinical relevance with clinical tumor response assessments [1,2,16].

The ordinary least squares (OLS) regression method is considered as the parameter estimation method of choice, since the standard Patlak model in Eq. 1 assumes a linear relationship between the measurements and the unknown parameters [16]. Moreover, note that Eq. 1 is only valid for $t > t^*$ which also corresponds to the multi-bed dynamic data acquisition time period ($t^* \cong$ 5-7min), i.e. with Patlak method early dynamic (TAC) data are not useful, except from the heart bed for the sole purpose of calculating the time integral of the input function [11]. Unlike Logan method [26], when the Patlak model formulation is applied [16,18] the need to measure the time integral of all voxel TACs across all tissues and beds is alleviated, making possible voxel-based estimation of K_i parameter from multi-bed dynamic PET data [11,19].

However, standard Patlak does not account for uptake reversibility (k_{loss} is assumed to be zero), resulting in underestimation of K_i when k_{loss} is non-negligible. Recently we introduced a generalized Patlak method which is non-linear and, thus, less robust to noise, but capable to account for non-negligible k_{loss} reversibility and, therefore, provide K_i estimates of higher quantitative accuracy (Eq. 2) [18,19]:

$$\begin{aligned} C(t) &= K_i \int_0^t e^{-k_{loss}(t-\tau)} C_p(t)d\tau + VC_p(t) \\ &= (K_i e^{-k_{loss}t}) * C_p(t) + VC_p(t),\ t > t^* \end{aligned} \quad (2)$$

The physiological parameter of net efflux rate constant k_{loss} depends on k_2, k_3 and k_4 parameters, according to Eq. (3) [19]:

$$k_{loss} = \frac{k_3}{k_3 + k_4}\frac{k_2 k_4}{k_2 + k_3} \quad (3)$$

An alternative graphical analysis method for estimation of reversible uptake rate constants could have been the Logan

method, which has been extensively used for reversible binding tracers in PET neuroimaging studies [26,27]. However, the generalized Patlak modeling scheme is capable not only of accounting for reversible uptake, unlike standard Patlak, but also retaining the benefit of Patlak formulations, which do not require integration of every voxel TAC but the input function, unlike Logan model [19,26].

For the non-linear estimation of the generalized Patlak parameters (K_i, k_{loss},V) we have proposed the application of the Basis Function Method (BFM), which utilizes a set of carefully selected basis functions to effectively linearize the estimation problem [19,30]. Due to high levels of noise present in the short dynamic PET frames of each bed, BFM produces highly noisy estimates particularly in low uptake and background regions. Thus, we have previously introduced the selective application of OLS regression to the voxels exhibiting low linear correlation to Patlak method, as they are more likely to be associated with high levels of noise to preserve robustness [19]. For the highly linear correlated voxels, often associated with low noise, BFM method can be applied to achieve superior accuracy. However, the threshold value defining the two voxel classes should be selected with care, as the quality in the parametric images may be affected. In general, a range of correlation threshold values of (0.85, 0.98) is recommended based on our findings in the current and previous studies [19].

C. Realistic 4D simulations of the Siemens Biograph mCT scanner

The *k*-parameter value set presented in Table I together with a 2-compartment 4-parameter kinetic model, the standard choice for FDG kinetic modeling (Fig. 2a), were employed to generate noise-free FDG TACs for a time range of 0-90min post-injection and a selection of types of tumors and normal tissues across the body (Table I and Fig. 2b). Later, the produced TACs were assigned to corresponding regions defined in the state-of-the-art digital anthropomorphic XCAT2 voxelized phantom to produce a set of 13 realistic dynamic noise-free image data, each corresponding to a different pass (Fig. 3).

Only the dynamic phantom image frames corresponding to the cardiac bed were constructed, as the simulation process is the same for the rest of the beds. However, it should be noted that the TACs assigned to each voxel of the cardiac bed were sampled exactly at mid-frame times determined by our proposed multi-bed dynamic PET data acquisition protocol for that particular bed, i.e. the time gaps between the frames of each bed were taken into account in our simulations [11].

Subsequently, the dynamic noise-free frames were forward projected and normalization, attenuation and scatter effects were added to simulate noise-free realistic projections. Moreover, PET system resolution response modeling was included in the forward projectors to match a FWHM spatial resolution of 4.5mm, using the e7tools (Siemens Healthcare) [31]. Subsequently, 15 realizations of quantitative levels of Poisson noise were added to each of the 13 noise-free dynamic sinograms to generate a total set of 13×15=195 3D sinograms. The level of Poisson noise was quantitatively determined for each frame by the dynamic activity distribution, the properties of Poisson distribution, the sensitivity of the mCT PET TOF scanner and the time duration of each frame. Subsequently, each of the generated noisy projections were reconstructed with an OP-OSEM algorithm (6 iterations total, 14 subsets) utilizing the e7tools reconstruction platform [31]. Finally, the technologies available on the mCT PET scanner, namely TOF acquisition and PSF modeling, were exploited for the enhancement of the whole-body parametric image quality [17,31,32].

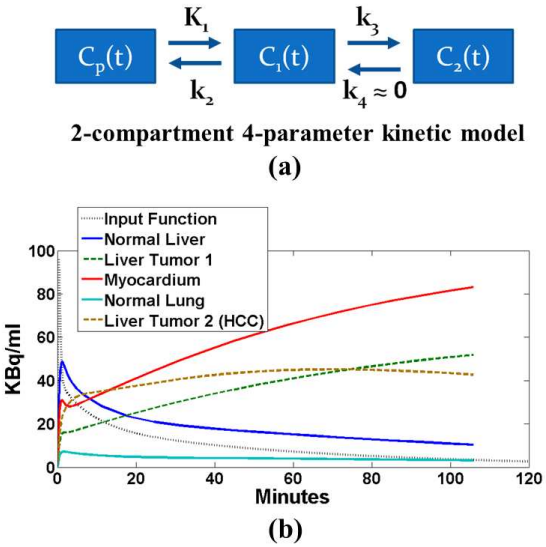

Fig. 2 (a) The standard full compartment kinetic model was employed in simulations, (b) noise-free (simulated) time-activity curves (TACs) as generated by the model (Fig. 2a) and the kinetic parameter values reviewed from literature (Table I)

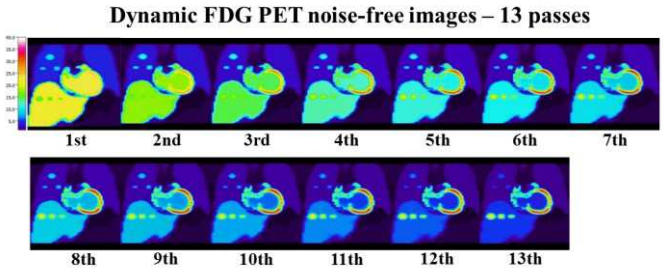

Fig. 3 Time sequence of dynamic PET noise-free image data. The single bed frames are generated using the XCAT phantom generation tool by sampling the noise-free FDG TACs (Fig 2b) at the times corresponding to a 13-pass whole-body dynamic PET acquisition.

The tumor region in Table I labeled as "liver tumor 2" or hepatocellular carcinoma HCC, with a k_4 parameter value being comparable to (approximately one third of) the respective k_3 value, is considered in this study as one characteristic case of a region with non-negligible FDG uptake reversibility (k_{loss}) [25]. Thus, it has been included in the simulations of this study with its quantitative evaluation presented in the results section. While k_4 may appear small as an absolute value, it is, in fact, not very small relative to k_3, and therefore may exhibit considerable net uptake

reversibility, appearing as a reduction in the TAC at later times ("liver tumor 2" TAC in Fig. 4a) [19]. However, the effect of a presence of non-negligible k_{loss} rate constant is more evident on the Patlak plots presented in Fig. 4b. The Patlak plots or curves are formed by points placed on a 2D diagram according to the dynamic PET measurements and their assumed relationship as described by the kinetic model equations (1) and (2) for the standard and generalized Patlak, respectively, and for $t>t^*$ [16,18,19].

If the standard Patlak assumptions are considered, but underlying k_{loss} is in fact non-negligible, then the second derivative of the Patlak plot with respect to the stretched time (variable in the x-axis) is no longer zero, as it would have been expected, and becomes negative, i.e. the Patlak plot "bends down" instead of being a straight increasing line [19]. The "bend down" effect results in underestimation of the slope of the straight fitted line (red lines), i.e. of K_i estimates, when using OLS regression on the bended Patlak plots.

However, under the generalized Patlak assumptions where k_{loss} can be non-zero (positive) but relatively small with respect to K_i, the same dynamic measurements now produce Patlak points falling across a nearly straight line and the true slope, or K_i, of the newly fitted lines is recovered (cyan and green fitted lines) [19]. The difference in the slope of the fitted lines between the true (noise-free) and noisy ROI-based measurements for each of the two Patlak models is attributed to the partial volume effect in the tumor regions [33].

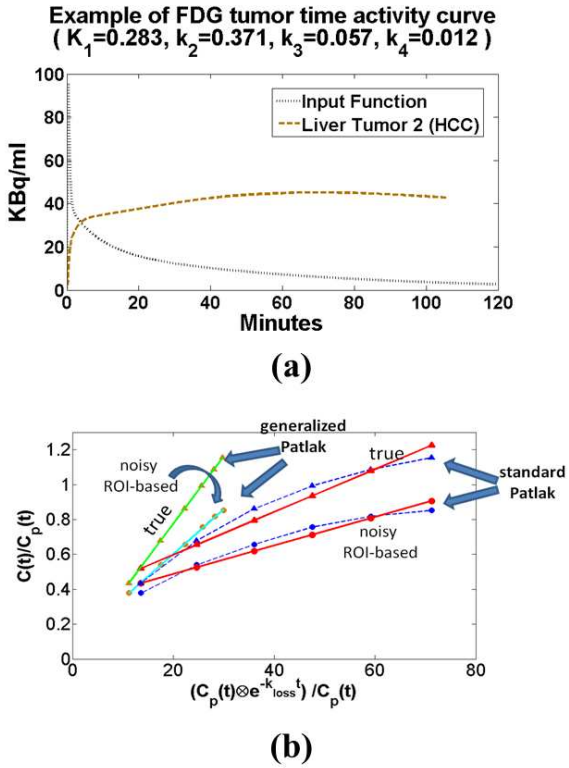

Fig. 4. (a) The input function and the noise-free TAC simulated from characteristic kinetic parameter values reported in literature [23-25] for a tumor case labeled as "liver tumor 2 HCC" in Table I. (b) Standard and Generalized Patlak plot curves and their corresponding fitted lines for noise-free and noisy ROI-extracted dynamic measurements from the region referenced in Fig. 4a

III. Results and Discussion

In Fig. 5, we present 8 sets of K_i images, each corresponding to a different position, from early to later time points with respect to injection time, of the incrementally shifted 6-pass acquisition time window. Each set of parametric images were estimated using either standard or hybrid Patlak generation algorithms, as applied on a set of reconstructed dynamic images, each belonging to the corresponding acquisition time-window. Moreover, the respective K_i images estimated from all available 13 passes/frames are shown as a reference case. Finally, this parametric image generation process has been applied both on noise-free and noisy simulated dynamic projection data, with the only other difference being that for the evaluation of the acquisition time-window effect on the generalized Patlak model the BFM estimation method was employed on the noise-free data, while the hybrid OLS/BFM method was applied on the noisy projections.

From the visual inspection of the estimated K_i images in Fig. 5, it can be observed that for the tumors located in the lung region of the XCAT phantom, where a non-negligible degree of uptake reversibility (k_{loss}) was simulated, the associated tumor-to-background (TBR) contrast is gradually reduced, in the case of standard Patlak modeling, as the 6-pass acquisition time-window moves to later time positions. A similar effect is observed when all 13 passes are included in the window.

For the generalized Patlak model, the noise-free data demonstrate a high contrast across all time-window positions even for the tumor associated with a non-negligible k_{loss} rate constant. This observation agrees with what is expected from the kinetic modeling theory described in previous sections. However, in the presence of high noise levels, mainly due to the short frame durations (45sec) of the proposed multi-bed dynamic acquisition protocol, hybrid Patlak K_i images also suffer from gradual TBR contrast degradation in the tumor regions with non-negligible uptake reversibility, though to a lesser extent compared to standard linear Patlak K_i images.

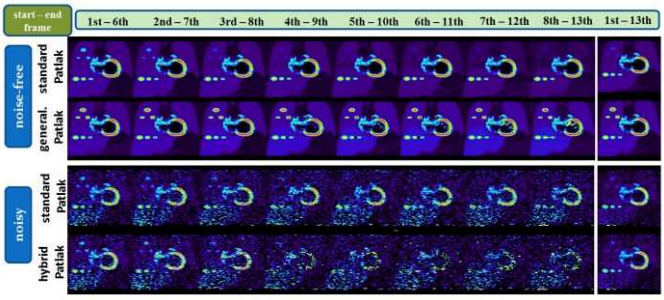

Fig. 5. Comparative evaluation of simulated K_i images for a range of acquisition time-windows. A threshold of 0.85 was applied for hybrid Patlak.

The quantitative evaluation of the bias in the K_i estimates from a simulated tumor region of non-negligible uptake reversibility is presented in Fig. 6a and b for the noise-free and noisy data respectively. The results clearly demonstrate that for both Patlak models, a minimum K_i bias was achieved when acquiring at the earliest time-window, with generalized (noise-

free case) and hybrid (noisy case) methods systematically achieving superior bias over the standard Patlak method.

Similarly, that acquisition window position resulted in the best tumor to background (TBR) contrast and contrast-to-noise ratio (CNR) scores over all the rest of the evaluated window positions (Fig. 7a and b). Again, hybrid Patlak imaging outperformed standard Patlak in nearly all cases and especially at the earliest time-window.

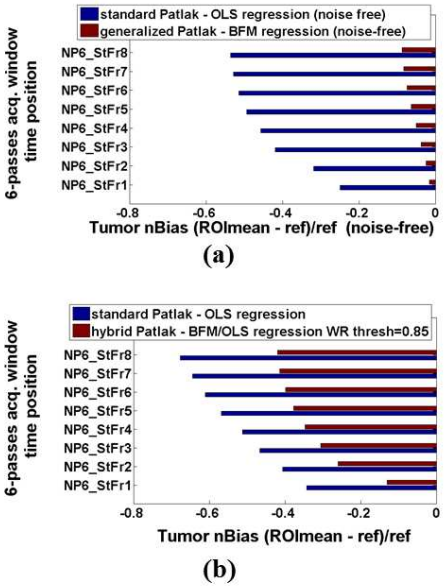

Fig. 6. Assessment of bias in the K_i images over a tumor region of non-negligible k_{loss} rate constant value for different positions of a 6-pass acquisition time-window and the two Patlak estimation methods for (a) noise-free and (b) noisy (20 realizations) simulated data.

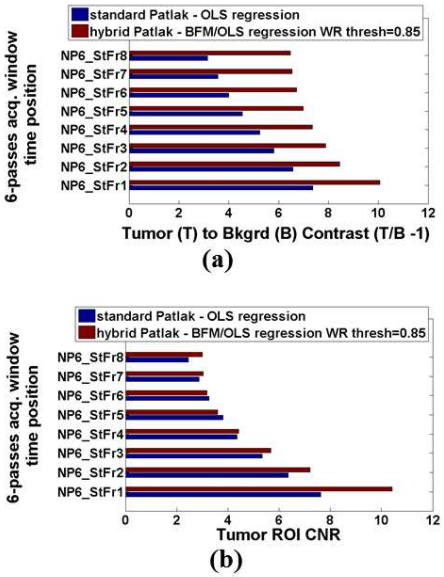

Fig. 7: Assessment of (a) tumor-to-background ratio (TBR constrast) and (b) Contrast-to-Noise ratio (CNR) in the K_i images over a liver tumor region for different time acquisition windows and the two Patlak estimation methods for noisy (20 realizations) simulated data.

However, unlike the noise-free case where the bias in the K_i estimates using exclusively the BFM method and the generalized Patlak model was always small, for the noisy data that observation was not repeated. On the contrary, at the presence of noise, where the hybrid OLS/BFM method had to be used, K_i bias approached the bias levels of standard Patlak method, as the window moved to later time points.

We attribute this behavior of hybrid K_i estimates under highly noisy conditions to the stronger effect of k_{loss} at later time frames, resulting in reduced counts for those frames (as demonstrated in Fig. 4a). The reduction in counts could further enhance noise levels at those frames, resulting in an overall reduction of the Patlak correlation coefficient of the TACs. Consequently, a higher number of voxel TACs is likely to now be associated with correlation coefficients lower than the predefined correlation threshold value of the hybrid Patlak algorithm [19]. As a result, more voxel TACs may now be classified as of "low Patlak correlation" and, consequently, standard Patlak assumptions and OLS regression will now be applied to more voxels of an image [19].

Thus, under highly noisy conditions, OLS method is expected to dominate over BFM in the context of hybrid Patlak imaging, causing the performance of the hybrid K_i images to resemble that of the standard Patlak K_i images. A potential strategy to avoid this problem is to reduce the correlation coefficient threshold to allow BFM to be applied to less correlated voxel TACs. However, this may further enhance noise in the K_i images, as BFM is less robust to noise [19]. Nevertheless, for the noisy case the bias of the hybrid OLS/BFM K_i images was always smaller than that of OLS K_i estimates, especially for the earliest time-window.

A clinical demonstration of the visual effect of the acquisition time-window position on whole-body K_i images from a 0-90min whole-body clinical study is illustrated in Fig. 8. In total, 7 positions are evaluated for the two Patlak methods.

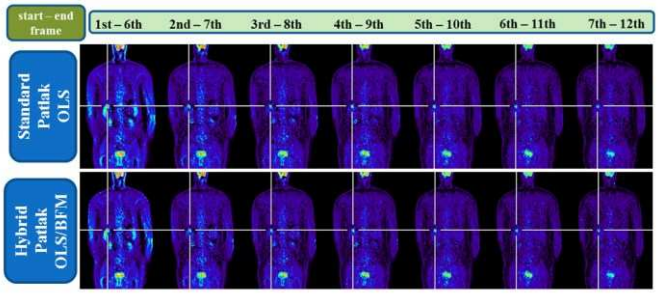

Fig. 8. Clinical demonstration of the impact of acquisition time-window position on whole-body parametric K_i imaging. In total, 7 sets of K_i images are presented, each corresponding to a different position of a 6-pass acquisition time-window. Both standard and hybrid Patlak image results evaluated.

Furthermore, Fig. 9 presents a quantitative analysis of the K_i bias over a lung tumor region for the same set of window positions and Patlak methods. For the bias calculation in the clinical images, where the ground truth is unknown, a hybrid K_i image, derived from all 13 passes, have been used as a reference value instead. Finally, Fig. 10 shows TBR and CNR

quantitative performance scores, as quantified over the same lung tumor region across the same clinical dataset.

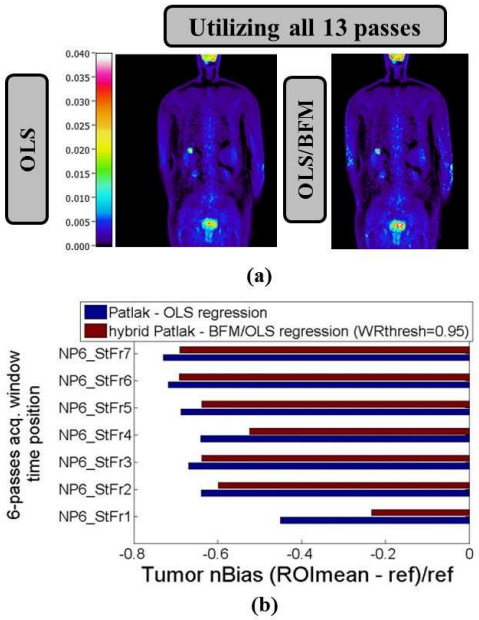

Fig. 9. (a) Clinical K_i whole-body images obtained after utilizing all available 13 whole-body passes: (top left) OLS and (top right) hybrid OLS/BFM images. (b) Absolute mean bias over a lung tumor region extracted from the same set of clinical K_i images. The impact of the time position of a fixed length (6 number of passes or NP6) acquisition time-window is evaluated for the two Patlak methods. The examined window positions are designated by the index of the starting frame (StFr) of every window. Bias has been calculated with respect to the hybrid K_i image of Fig 9a, top right.

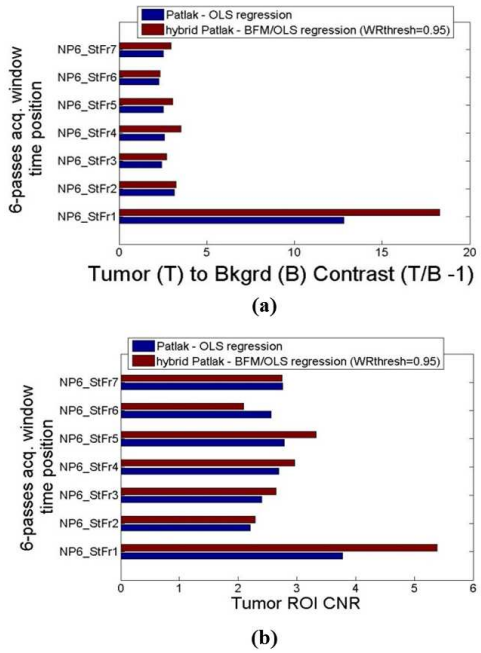

Fig. 10. Quantitative evaluation over a lung tumor region, as extracted from clinical whole-body parametric K_i images, of the impact of acquisition time-window position on (a) TBR contrast and (d) CNR. The examined window positions are designated by the index of the starting frame (StFr) of every window. Two Patlak methods have been evaluated for each window.

For both standard and generalized Patlak, the earliest acquisition time-window achieved the minimum K_i bias, as well as the highest TBR and CNR scores. Moreover, for that particular time window position, as well as for most of the other evaluated time-shifted acquisitions, hybrid Patlak K_i imaging outperformed standard Patlak for all the clinical data examined, suggesting the presence of some degree of uptake reversibility in the human FDG kinetics.

Therefore, we recommend applying the first acquisition window with the hybrid Patlak method.

IV. Conclusions and Future Prospects

In this study, we evaluated the quantitative impact of the position, relative to injection time, of a fixed-length (6-passes) multi-bed dynamic acquisition time-window on the whole-body parametric Ki images using both realistic simulated data with characteristic kinetics obtained from literature as well as real patient data.

In both simulation and clinical studies, we concluded that, regardless of the Patlak model used, the earliest acquisition time-window achieved the best quantitative performance in terms of bias, TBR contrast and CNR metrics of the final K_i parametric images. Furthermore, we have demonstrated the higher quantitative accuracy in tumor regions for the generalized Patlak model and the hybrid Ki imaging algorithm. At the same time, we have also discussed their limitations at high levels of noise, where the standard Patlak model may still be a robust parametric imaging solution, with satisfactory accuracy, provided the earliest time-window is selected.

Our conclusions were based not only on simulated TACs where the uptake reversibility was "imposed", based on literature review, but also on actual clinical studies, which reproduced our simulation results, suggesting the real presence of some degree of FDG uptake reversibility. In addition, our findings demonstrate the importance of acquisition time-window optimization in dynamic PET studies, especially when conducted over multiple bed positions, by taking into account very important parameters such as the kinetic properties of the PET tracer, the assumptions of the kinetic model employed and the model robustness to high levels of noise usually present in dynamic, especially whole-body, PET studies.

In the future, we plan to utilize our developed direct 4D whole-body PET parametric imaging methods to investigate if they can potentially provide further margins of optimization in the currently proposed acquisition protocols [13,14]. Our ultimate aim through such acquisition optimization studies is to sufficiently demonstrate that whole-body parametric PET imaging can be clinically feasible and may offer high quantitative potential, provided that it is optimized such as to maximize the amount of possible information content that can be delivered to the clinician, given the limited acquisition time available in the clinic.

V. Acknowledgments

The authors would like to gratefully acknowledge support by Siemens Medical Solutions and the Swiss National Science Foundation under Grant SNSF 31003A-149957. We also wish to thank Dr. Fotis A. Kotasidis for discussions regarding the the effect of uptake reversibility often observed in dynamic PET FDG studies.

References

[1] C. Messa, Y. Choi, C.K. Hoh, E.L. Jacobs, J.A. Glaspy, S. Rege, E. Nitzsche, S. C. Huang, M. E. Phelps, and R. A. Hawkins, "Quantification of glucose utilization in liver metastases: parametric imaging of FDG uptake with PET," J. of Comp. Assist. Tomography, vol. 16, no. 5, p. 684, 1992

[2] K. R. Zasadny and R. L. Wahl "Enhanced FDG-PET tumor imaging with correlation-coefficient filtered influx-constant images," J. Nucl. Med., 37(2), p. 371-374, 1996

[3] I. C. Smith, A. E. Welch, A. W. Hutcheon, I. D. Miller, S. Payne, F. Chilcott, S. Waikar, T. Whitaker, A. K. Ah-See, O. Eremin, S. D. Heys, F. J. Gilbert and P. F. Sharp, "Positron emission tomography using [18F]-fluorodeoxy-D-glucose to predict the pathologic response of breast cancer to primary chemotherapy," J. Clin. Onc., 18(8), 1676-1688, 2000

[4] D. Thorwarth, S. M. Eschmann, F. Paulsen and M. Alber, "A kinetic model for dynamic [18F]-Fmiso PET data to analyse tumour hypoxia," Phys. Med. Biol., 50(10), p. 2209, 2005

[5] T. Schroeder, M. F. V. Melo, G. Musch, R. S. Harris, T. Winkler, and J. G. Venegas "PET imaging of regional 18F-FDG uptake and lung function after cigarette smoke inhalation," J. Nucl. Med., 48(3), p. 413-419, 2007

[6] A. Dimitrakopoulou-Strauss, L. Pan, and L. G. Strauss, "Parametric imaging: a promising approach for the evaluation of dynamic PET-18 F-FDG studies-the DKFZ experience," Hel. J. Nucl. Med., 13(1), p. 18-22, 2010

[7] W. Wang, N. Y. Lee, J. C. Georgi, M. Narayanan, J. Guillem, H. Schöder and J. L. Humm, "Pharmacokinetic analysis of hypoxia 18F-fluoromisonidazole dynamic PET in head and neck cancer," J. Nucl. Med., 51(1), p. 37-45, 2010

[8] D. J. Apostolopoulos, A. Dimitrakopoulou-Strauss, P. Hohenberger, S. Roumia and L. G. Strauss, "Parametric images via dynamic 18F-fluorodeoxyglucose positron emission tomographic data acquisition in predicting midterm outcome of liver metastases secondary to gastrointestinal stromal tumours," Eur. J. Nucl. Med. Mol. Imaging, 38(7), p. 1212-1223, 2011

[9] N. A. Karakatsanis, M. A. Lodge, Y. Zhou, J. Mhlanga, M. Chaudhry, A. K. Tahari, R. L. Wahl and A. Rahmim, "Towards parametric whole-body FDG PET/CT imaging: potentials for enhanced tumor detectability," J. Nucl. Med. 2012; 53 (Supplement 1):1236, 2012

[10] G. Tomasi, F. Turkheimerand E. Aboagye, "Importance of quantification for the analysis of PET data in oncology: review of current methods and trends for the future," Mol. Imag. Biol., 14(2), p. 131-146, 2012

[11] N. A. Karakatsanis, M. A. Lodge, A. K. Tahari, Y. Zhou, R. L. Wahl and A. Rahmim, "Dynamic whole-body PET parametric imaging: I. Concept, acquisition protocol optimization and clinical application," Phys. Med. Biol. 58(20), p. 7391, 2013

[12] N. A. Karakatsanis, M. A. Lodge, Y. Zhou, R. L. Wahl and A. Rahmim, "Dynamic whole-body PET parametric imaging: II. Task-oriented statistical estimation," Phys. Med. Biol. 58(20), p. 7419, 2013

[13] N. A. Karakatsanis, M. A. Lodge, R. L. Wahl and A. Rahmim, "Direct 4D whole-body PET/CT parametric image reconstruction: concept and comparison vs. indirect parametric imaging," J. Nucl. Med. 2013; 54 (Supplement 2):2133, 2013

[14] N. A. Karakatsanis and A. Rahmim, "Whole-body PET parametric imaging employing direct 4D nested reconstruction and a generalized non-linear Patlak model," Proc. SPIE 9033, Medical Imaging 2014: Physics of Medical Imaging, 90330Y, 2014

[15] N. A. Karakatsanis, M. A. Lodge, Y. Zhou, J. Mhlanga, M. A. Chaudhry, A. K. Tahari, R. L. Wahl and A. Rahmim, "Dynamic multi-bed FDG PET imaging: feasibility and optimization," Nuclear Science Symposium and Medical Imaging Conference (NSS/MIC), Valencia, Spain, p. 3863-3870, 2011

[16] C. S. Patlak, R. G. Blasberg, and J. D. Fenstermacher, "Graphical evaluation of blood-to-brain transfer constants from multiple-time uptake data," J. Cereb. Blood Flow Metab., 3(1), p. 1-7, 1983

[17] K. A. Krohn, D. A. Mankoff, M. Muzi, J. M. Link and A. M. Spence, "True tracers: comparing FDG with glucose and FLT with thymidine," Nucl. Med. Biol., 32(7), p. 663-671, 2005

[18] C. S. Patlak and R. G. Blasberg, "Graphical evaluation of blood-to-brain transfer constants from multiple-time uptake data. Generalizations," J. Cereb. Blood Flow Metab., 5, p. 584, 1985

[19] N. A. Karakatsanis, Y. Zhou, M. A. Lodge, M. E. Casey, R. L. Wahl and A. Rahmim, "Quantitative whole-body parametric PET imaging incorporating a generalized Patlak model," Nuclear Science Symposium and Medical Imaging Conference (NSS/MIC), Seoul, S. Korea, 2013

[20] G. A. Sayre, B. L. Franc and Y. Seo "Patient-specific method of Generating Parametric Maps of Patlak K_i without Blood Sampling or Metabolite Correction: A Feasibility Study.", Int. J. Mol. Imag., 2011.

[21] C. K. Hoh, D. Vera and C. Schiepers, "Reducing effects of non-zero k_4 and metabolites in generating Patlak parametric images of FLT uptake," J. Nucl. Med.; 52 (Supplement 1): 2063, 2011

[22] B.W. Jakoby, Y. Bercier, M. Conti, M.E. Casey, B. Bendriem and D.W. Townsend "Physical and clinical performance of the mCT time-of-flight PET/CT scanner," Phys. Med. Biol., 56(8), p.2375, 2011

[23] A. Dimitrakopoulou-Strauss, V. Georgoulias, M. Eisenhut, F. Herth, S. Koukouraki, H. Macke, U. Haberkorn, and L. Strauss, "Quantitative assessment of SSTR2 expression in patients with non-small cell lung cancer using 68 Ga-DOTATOC PET and comparison with 18 F-FDG PET," Eur. J. Nucl. Med. and Mol. Imaging, vol. 33, no. 7, p. 823–830, 2006.

[24] S. Okazumi, A. Dimitrakopoulou-Strauss, M. Schwarzbach, and L. Strauss, "Quantitative, dynamic 18F-FDG-PET for the evaluation of soft tissue sarcomas: relation to differential diagnosis, tumor grading and prediction of prognosis," Hel. J. Nucl. Med., vol. 12, no. 3, p. 223, 2009

[25] T. Torizuka, N. Tamaki, T. Inokuma, Y. Magata, S. Sasayama, Y. Yonekura, A. Tanaka, Y. Yamaoka, K. Yamamoto, J. Konishi et al., "In vivo assessment of glucose metabolism in hepatocellular carcinoma with FDG-PET," J. Nucl. Med., vol. 36, no. 10, p. 1811, 1995.

[26] R. E. Carson, "Tracer kinetic modeling in PET," Positron Emission Tomography, Springer London, Book Chapter, p. 127-159, 2005

[27] H. Zaidi, "Tracer kinetic modeling in PET," PET Clinics, 2(2), p. 267-277, 2007

[28] J. Logan, J. S. Fowler, N. D. Volkow, A. P. Wolf, S. L. Dewey, D. J. Schlyer, R. R. MacGregor, R. Hitzemann, B. Bendriem, S. J. Gatley and D. R. Christman, "Graphical analysis of reversible radioligand binding from time-activity measurements applied to [N-11C-methyl]-(-)-cocaine PET studies in human subjects," J. Cereb. Blood Flow Metab., ,10(5), 740-747, 1994

[29] J. Logan, "Graphical analysis of PET data applied to reversible and irreversible tracers," Nucl. Med. Biol., 27(7), p. 661-670, 2000

[30] R. N. Gunn, A. A. Lammertsma, S. P. Hume and V. J. Cunningham, "Parametric imaging of ligand-receptor binding in PET using a simplified reference region model," Neuroimage, 6(4), p. 279, 1997

[31] V. Y. Panin, F. Kehren, C. Michel and M. E. Casey "Fully 3-D PET reconstruction with system matrix derived from point source measurements," IEEE Trans. in Med. Imag., 25(7), p. 907-921, 2006

[32] N. A. Karakatsanis, A. Rahmim, M. A. Lodge and H. Zaidi, "Introducing Time-of-Flight and Resolution Recovery Image Reconstruction to Whole-body PET Parametric Imaging," Nuclear Science Symposium and Medical Imaging Conference (NSS/MIC), Seattle, WA, USA, 2014

[33] M. Soret, S. L. Bacharach and I. Buvat, "Partial-volume effect in PET tumor imaging," J. Nucl. Med., 48(6), p. 932-945, 2007